# Changes in biomass burning, wetland extent, or agriculture drive atmospheric $NH_3$ trends in key African regions

Jonathan E. Hickman[1*], Niels Andela[2†], Enrico Dammers[3], Lieven Clarisse[4], Pierre-François Coheur[4], Martin Van Damme[4], Courtney Di Vittorio[5], Money Ossohou[6], Corinne Galy-Lacaux[7], Kostas Tsigirdis[1,8], Susanne Bauer[1]

[1]NASA Goddard Institute for Space Studies, New York, USA

[2]NASA Goddard Space Flight Center, Beltsville, USA

[3]Air Quality Research Division, Environment and Climate Change Canada, Toronto, Canada

[4]Université libre de Bruxelles (ULB), Service de Chimie Quantique et Photophysique, Atmospheric Spectroscopy, Brussels, Belgium

[5] Wake Forest University, Winston-Salem, USA

[6]Laboratoire des Sciences de la Matière, de l'Environnement et de l'Energie Solaire, Université Félix Houphouët-Boigny, Abidjan, Côte d'Ivoire

[7]Laboratoire d'Aérologie, Université Toulouse III Paul Sabatier / CNRS, France

[8]Columbia University, New York, USA

[†]Now at School of Earth and Ocean Sciences, Cardiff University, Cardiff, UK

*_Correspondence to_: jonathan.e.hickman@nasa.gov

**Abstract**

Atmospheric ammonia ($NH_3$) is a precursor to fine particulate matter and a source of nitrogen (N) deposition that can adversely affect ecosystem health. The main sources of $NH_3$—agriculture and biomass burning—are undergoing or expected to undergo substantial changes in Africa. Although evidence of increasing $NH_3$ over parts of Africa has been observed, the mechanisms behind these trends are not well understood. Here we use

observations of atmospheric $NH_3$ vertical column densities (VCDs) from the Infrared Atmospheric Sounding Interferometer (IASI) along with other satellite observations of the land surface and atmosphere to evaluate how $NH_3$ concentrations have changed over Africa from 2008 through 2018, and what has caused those changes. In West Africa $NH_3$ VCDs are observed to increase during the late dry season, with increases of over 6% $yr^{-1}$ in Nigeria during February and March ($p<0.01$). These positive trends are associated with increasing burned area and CO trends during these months, likely related to agricultural preparation. Increases are also observed in the Lake Victoria Basin, where they are associated with expanding agricultural area. In contrast, $NH_3$ VCDs declined over the Sudd wetlands in South Sudan by over 1.5% $yr^{-1}$, though not significantly ($p=0.28$). Annual maxima in $NH_3$ VCDs in South Sudan occur during February through May and are associated with drying of temporarily flooded wetland soils, which favor emissions of $NH_3$. The change in mean $NH_3$ VCDs over the Sudd is strongly correlated with variation in wetland extent in the Sudd: in years when more area remained flooded during the dry season, $NH_3$ concentrations were higher ($r=0.64$, $p<0.05$). Relationships between biomass burning and $NH_3$ may be observed when evaluating national-scale statistics: countries with the highest rates of increasing $NH_3$ VCDs also had high rates of growth in CO VCDs; burned area displayed a similar pattern, though not significantly. Livestock numbers were also higher in countries with intermediate or high rates of $NH_3$ VCD growth. Fertilizer use in Africa is currently low but growing; implementing practices that can limit $NH_3$ losses from fertilizer as agriculture is intensified may help mitigate impacts on health and ecosystems.

## 1. Introduction:

Ammonia ($NH_3$), a reactive nitrogen (N) trace gas, plays a number of important roles in the atmosphere, with implications for human health, climate, and ecosystems. Once in the atmosphere, $NH_3$ contributes to the production of inorganic aerosols, the primary constituents of fine particulate matter and a serious health hazard (Bauer et al., 2016; Lelieveld et al., 2015; Pope et al., 2002). $NH_3$ can also be deposited to downwind ecosystems, contributing to eutrophication, soil acidification, vegetation damage, productivity declines, reductions in biodiversity, and indirect greenhouse gas emissions

(Denier Van Der Gon and Bleeker, 2005; Krupa, 2003; Matson et al., 1999; Stevens et al., 2018; Tian and Niu, 2015).

Although $NH_3$ is emitted from natural soils, agriculture is by far the largest source of $NH_3$ globally (Behera et al., 2013; Bouwman et al., 1997). Urea fertilizer and livestock excreta are particularly important substrates for $NH_3$ formation, and can be volatilized quickly under favorable environmental conditions (Bouwman et al., 1997). In all soils, $NH_3$ is formed in solution following the dissociation of ammonium ($NH_4^+$; Eq. 1).

$$NH_4^+ + OH^- \leftrightarrow H_2O + NH_3 \qquad \text{(Eq. 1)}$$

Soil $NH_3$ production is temperature-dependent, doubling with every 5°C temperature increase, though the actual soil $NH_3$ flux is determined in part by plant and soil physiological and physical factors (Sutton et al., 2013). On average, fertilizer use has been extremely low in sub-Saharan Africa—often an order of magnitude or more lower than typical in Europe, the United States, or China (Hazell and Wood, 2008; Vitousek et al., 2009). Livestock manure N content also tends to be very low in sub-Saharan Africa (Rufino et al., 2006). The low fertilizer use suggests that natural soils (as opposed to agricultural soils) may be a more important source in the region than elsewhere in the world. However, agricultural intensification and increasing fertilizer use has been a central policy focus for many African countries, with national and regional efforts to increase N inputs by an order of magnitude or more (AGRA, 2009).

After agriculture, biomass burning is the most important source of $NH_3$ globally (Bouwman et al., 1997), with roughly 60 to 70% of global $NH_3$ emissions from fires occurring in Africa (Cahoon et al., 1992; Whitburn et al., 2015). The amount of $NH_3$ emitted from biomass fires is controlled primarily by the type of burning that occurs. N in fuel is present predominantly in a chemically reduced state, and $NH_3$ is emitted in greater quantities from low temperature smoldering combustion in which fuel N is incompletely oxidized (Goode et al., 1999; Yokelson et al., 2008). Fuel moisture content, which can help determine whether combustion is smoldering or flaming, is thus an important determinant of biomass burning $NH_3$ emissions (Chen et al., 2010).

In contrast to other reactive N gases such as $NO_x$ (nitric oxide + nitrogen dioxide), $NH_3$ emissions are typically unregulated outside of Europe (Anker et al., 2018; Kanter, 2018; USDA Agricultural Air Quality Task Force, 2014), and substantial increasing trends have been observed by the NASA Atmospheric InfraRed Sounder (AIRS) and the Infrared Atmospheric Sounding Interferometer (IASI) over many of the world's major agricultural and biomass burning regions during the 21st century (Van Damme et al., 2021; Warner et al., 2017). West Africa has been identified as an important $NH_3$ source region (Van Damme et al., 2018), where a trend of increasing $NH_3$ concentrations in recent decades has been attributed at least in part to increased fertilizer use (Van Damme et al., 2021; Warner et al., 2017). Increasing trends have also been observed over central Africa, and attributed to higher rates of biomass burning (Van Damme et al., 2021; Warner et al., 2017). However, the studies by Warner et al. (2017) and Van Damme et al. (2021) were global in nature, and as such could not include detailed explorations of the drivers of trends such as consideration of emission seasonality or the geographic distribution of emission drivers. Consideration of these factors is particularly important across large parts of Africa where both biomass burning and soils are potentially important sources of $NH_3$ (van der A et al., 2008).

Here we use an eleven-year satellite record to evaluate trends in atmospheric $NH_3$ concentrations over Africa from 2008 through 2018, including detailed examination of three regions where changes are pronounced: West Africa, the Lake Victoria Region, and South Sudan.

## 2. Data and Methods

### 2.1 Global gridded data

Multiple data products were used, including satellite observations and spatial datasets:

-IASI-A, launched aboard the European Space Agency's MetOp-A in 2006, provides measurements of atmospheric $NH_3$ and carbon monoxide (CO) twice a day (9:30 in the morning and evening, Local Solar Time at the equator). Here we use morning observations, when the thermal contrast is more favorable for retrievals (Clarisse et al., 2009; Van Damme et al., 2014a). The $NH_3$ retrieval product used (ANNI-$NH_3$-v3R) follows a neural

network retrieval approach. We refer to Van Damme et al. (2017) and Van Damme et al. (2021) for a detailed description of the algorithm. For CO, we used the product obtained with the FORLI v20140922 retrieval algorithm (Hurtmans et al., 2012). Given the absence of hourly or even daily observations of $NH_3$ concentrations in sub-Saharan Africa, the detection limit of IASI is difficult to determine with certainty. However, the region experiences high thermal contrast, and IASI seems to be able to reliably observe $NH_3$ down to 1 to 2 ppb at the surface (Clarisse et al., 2009; Van Damme et al., 2014b). We gridded the Level-2 IASI $NH_3$ and CO products to 0.5° × 0.5° resolution. We used a conventional binning approach based on the center of each satellite footprint. We did not apply an averaging weight. Quality control procedures were followed as detailed in van Damme et al. 2017 and Van Damme et al., 2021. Specifically, the screening of retrievals included filtering of retrievals where cloud cover is over 10%, where the total column density is below zero and the absolute value of the hyperspectral range index (HRI) is above 1.5, and where the ratio of the total column density to HRI is larger than $1.5 \times 10^{16}$ molecules $cm^{-2}$.

The IASI products have been validated using ground-based Fourier transform infrared (FTIR) observations of $NH_3$ total columns, with robust correlations at sites with high $NH_3$ concentrations, but lower at sites where atmospheric concentrations approach IASI's detection limits (Dammers et al., 2016; Guo et al., 2021). Compared to the FTIR observations, total columns from previous IASI $NH_3$ products (IASI-LUT and IASI-NNv1) are biased low by ~30% which varies per region depending on the local concentrations. Although FTIR observations are absent from Africa, earlier work has shown fair agreement between previous versions of IASI total column densities and surface observations of $NH_3$ using passive samplers across the International Network to study Deposition and Atmospheric chemistry in AFrica (INDAAF) network in West Africa (Van Damme et al., 2015), including in observations of seasonal variation (Hickman et al., 2018; Ossohou et al., 2019). Validation of the IASI CO product using surface, aircraft, and satellite observations have found total columns to have an error that is generally below 10-15% in the tropics and mid-latitudes (George et al., 2009; Kerzenmacher et al., 2012; Pommier et al., 2010; De Wachter et al., 2012). The IASI $NH_3$ and CO products were used for the years 2008—the first full year of data available—to the end of 2018. Random errors in observations can be

assumed to cancel out in the annual mean, which is what we used in our analysis. With the assumption that random errors cancel out, only systematic errors related to tropospheric vertical column contents remain; these systematic errors do not contribute to uncertainty in trend analyses. In addition, we first take monthly averages based on all daily observations within a given month before calculating seasonal means to minimize any potential effects of temporal variability in cloud cover.

-The Tropical Rainfall Measuring Mission (TRMM) daily precipitation product (3B42) is based on a combination of TRMM observations, geo-synchronous infrared observations, and rain gauge observations (Huffman et al., 2007). Independent rain gauge observations from West Africa have been used to validate the product, with no indication of bias in the product (Nicholson et al., 2003).

- NOAA Global Surface Temperature Dataset, a 0.5° gridded 2m monthly land surface temperature product (Fan and van den Dool, 2008). The data set is based on a combination of station observations from the Global Historical Climatology Network version 2 and the Climate Anomaly Monitoring System (GHCN_CAMS), and uses an anomaly interpolation approach which relies on observation-based reanalysis data to derive spatio-temporal variation in temperature lapse rates for topographic temperature adjustment.

- 500m MCD64A1 collection 6 Moderate Resolution Imaging Spectroradiometer (MODIS) burned area product for the period 2008-2018 (Giglio et al., 2018). The burned area data are aggregated by month and gridded to 0.25° resolution, and do not include burned area from small fires.

- MODIS MCD12C1 (collection 5) land cover product, which provides the percentage of cropped area in each 0.25° grid cell (Friedl et al., 2002). In Africa, agriculture is often practiced in complex mosaics of agricultural and natural land cover, so we used both the crop and crop/natural area mosaic MODIS classifications as agricultural area in our analysis.

-We also used data on the spatio-temporal distribution of armed conflict events from the Armed Conflict Location & Event Data Project (ACLED; Raleigh et al., 2010). We included data for both violent and non-violent conflict events over the period 2008-2018.

## 2.2 Sudd wetland extent

Monthly flooded area extents of the Sudd Wetland, South Sudan from 2000 to 2017 were derived from 8-day composite MODIS land surface reflectance imagery (MOD09A1); data from 2005 through 2017 were used in the analyses. We refer to Di Vittorio and Georgakakos (2018) for a detailed description of the classification procedure designed to retrieve these data. In summary, monthly flood maps were obtained through a two-stage classification procedure. The first stage used the full 18-year data set to produce a wetland land cover map that distinguishes between wetland vegetation classes and their flooding regimes (permanently flooded, seasonally flooded, or non-flooded). The second stage compares seasonally flooded pixels from each vegetation class to their non-flooded counterparts on a monthly basis to identify the timing and duration of flooding for each pixel. These data were originally derived to calibrate a hydrologic model of the Sudd that is dependent on Nile flows; therefore, a connectivity algorithm was applied to ensure that all flooded pixels were physically connected to the Nile River. A few adjustments have been made to the previously published dataset for the application of this study. The classification algorithm has been improved to more accurately capture the inter-annual fluctuations in the permanently flooded areas. The dataset was also extended through 2017, and the total flooded area was quantified prior to applying the connectivity algorithm. The magnitudes of the monthly flooded area estimates are now substantially larger because they include areas flooded from local runoff in addition to areas flooded by the Nile River.

## 2.3 Spatial and national analyses

We evaluated spatial relationships between mean annual tropospheric $NH_3$ concentration and several independent variables at 0.25° resolution: population density, livestock density, and cropped area. Population density and livestock density data are not available as time series suitable for trend analysis, so we use single year values in our analyses. We calculated population density based on the 2017 version of the US Department of Energy's Gridded Landscan population dataset (Dobson et al., 2000;

available at https://landscan.ornl.gov). Livestock density was based on the FAO global gridded livestock dataset for the year 2007 (Robinson et al., 2014). Before analysis, we converted the livestock densities of chickens, goats, pigs, and sheep to tropical livestock units (TLU), using values of 0.01, 0.1, 0.2, and 0.1 TLU, respectively; North African cattle were converted using a factor of 0.7, whereas sub-Saharan cattle were converted using a factor of 0.5 (Chilonda and Otte, 2006). For cropped area, we used the MODIS MCD12C1 (collection 5) land cover product as described above. We conducted spatial analyses by establishing a map of 3° grid cells and calculating the correlation between the value of each independent variable and $NH_3$ for all 0.5° grid cells within the larger grid cells (N = 36 including water grid cells, though these were excluded from the analysis).

National data on annual livestock numbers, crop production, and fertilizer N use were obtained from the UN Food and Agriculture Organization FAOSTAT for 51 African countries (FAO, 2020). Livestock data consisting of sheep, goats, cattle, and pigs were converted to tropical livestock units as described above, and buffaloes were converted using a conversion factors of 0.7 (Chilonda and Otte, 2006). National emissions of $CO_2$ were obtained from World Bank Open Data (World Bank, 2019). National-level mean annual cropland area, burned area, and atmospheric $NH_3$ and CO concentrations were also calculated for each of the 51 countries from the spatial datasets described above. Countries were sorted into three bins based on whether their relative change in mean annual $NH_3$ concentration was low, medium or high, and means and standard errors were calculated for each of the three 17-country bins.

Linear trend analyses were conducted using linregress from the scipy.stats package in Python v3.6.3. Statistical analyses of national scale data were conducted using ANOVA in R. Data were log or rank transformed when necessary to meet the assumptions of ANOVA. Values of $\alpha$ for treatment comparisons following significant ANOVA results were corrected for multiple testing using Benjamini-Hochberg corrections.

## 3. Results & Discussion

### 3.1 Continental distributions and trends

Mean annual $NH_3$ concentrations for 2008-2018 are highest across the savannas and forest-savanna mosaics in North equatorial Africa, and especially in West Africa; there are smaller regional hotspots in the Lake Victoria basin, South Sudanese wetlands, and along the Nile delta and river (Fig. 1a). Parts of these regions experience substantial biomass burning (Fig. 1e), high livestock densities (Fig. 1g), and/or high cropland cover (Fig. 1h), all of which can contribute to $NH_3$ emissions. The high concentrations in West Africa, which is one of the major global $NH_3$ hotspots (Van Damme et al., 2018), is likely the result of biomass burning emissions. Biomass burning emissions tend to drive seasonal variation in $NH_3$ VCDs in West Africa, with the largest emissions occurring late in the dry season and early rainy season (Hickman et al., 2021b). In addition to local emissions, biomass burning emissions and their reactive products are transported to the coast of West Africa during both the northern hemisphere rainy season, when it is transported from central and southern Africa, and during the dry season, when it is transported from biomass burning regions to the east (Sauvage et al., 2007). Most areas with trends are significant at P=0.2 or higher (Fig. S1).

In addition to being hotspots of mean $NH_3$ concentrations, some of these regions have also experienced increases in $NH_3$ concentrations from 2008 to 2018 (Fig. 1b). Like Warner et al. (2017) and Van Damme et al. (2021), we observed some increases in the northern grasslands, central African forests, and the Nile region, but we also observe trends in the Lake Victoria Basin, which Warner et al. (2017) did not, but Van Damme et al. (2021) did. Also in contrast to Warner et al. (2017) but in line with Van Damme et al. (2021), we observe a prominent decline in $NH_3$ VCDs over South Sudan (Fig. 1b, S1).

The Nile region exhibits elevated $NH_3$ concentrations and a modest positive trend over the observation period (Fig. 1a, 1b). This trend appears largely to be related to agriculture and livestock: in a spatial analysis, snapshots of livestock densities and of population densities are both positively related to changes in $NH_3$ VCDs (Fig. 2). Although there is not a positive relationship between agricultural area and $NH_3$ VCDs over the Nile region from 2008 to 2018, Egypt's population increased by roughly 25% over that period (World Bank, 2019), and fertilizer N use increased by roughly 8% after a decline in use

between 2004 and 2007 (FAO, 2020), suggesting that increased agricultural N inputs may be contributing to the trend. We evaluate the other regions in more detail below.

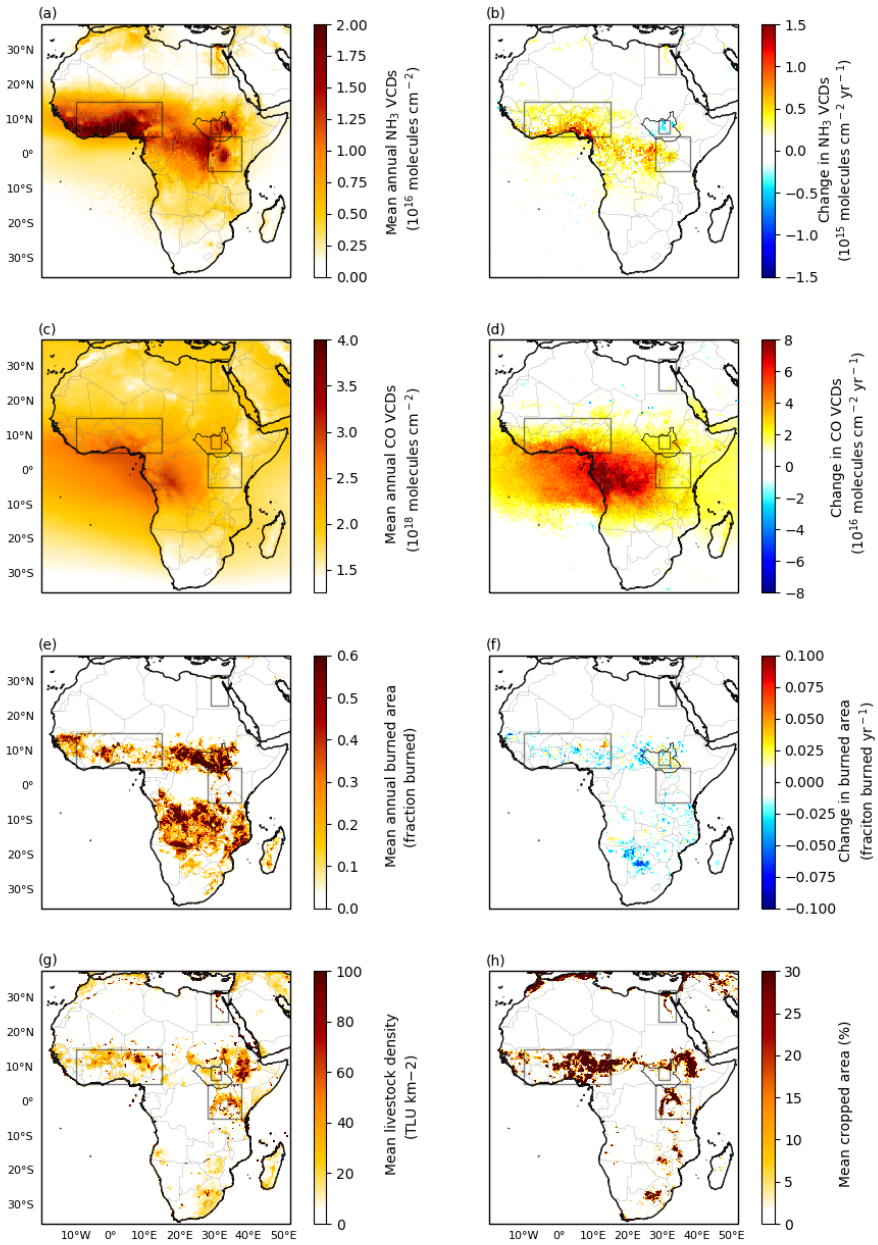


**Figure 1.** Annual averages and trends in atmospheric $NH_3$ VCDs, CO VCDs, and burned area, as well as spatial distribution of livestock density and cropped area across seven sub-Saharan African ecoregions. Mean annual (a) and trend (b) in atmospheric $NH_3$ VCDs from

IASI for the period 2008 through 2018. Mean annual (c) and trend (d) in annual atmospheric CO VCDs from IASI for the same period. Mean annual (e) and trend (f) in annual burned area from MODIS for 2008-2018. Livestock densities for 2007 from the FAO (f), and mean cropped area from MODIS for 2008-2018 (g). The border of South Sudan is highlighted in black, and several regions boxed: the Nile region at 30°N, the Sudd wetland in South Sudan, the Lake Victoria region at the equator, and West Africa centered around 10°N.

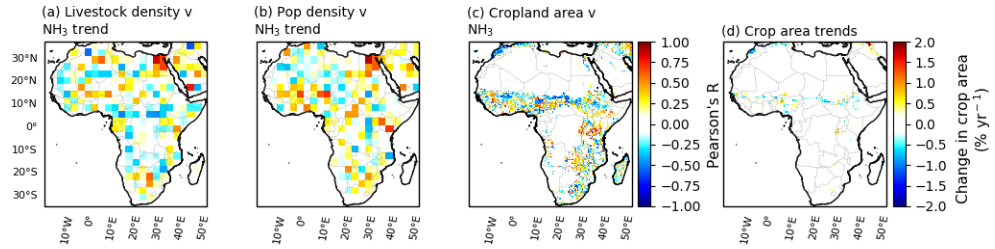


**Figure 2.** Relationships between $NH_3$ trends and livestock density, population density, and cropland area, as well as changes in cropland area. Spatial correlations between changes in annual atmospheric $NH_3$ VCDs and livestock density (a) and population density (b). Correlation between cropland area and $NH_3$ VCDs for 2008 through 2018 (c). Change in crop area for 2008 through 2018 (d). The $NH_3$ and crop area trends are based on data for 2008 through 2018, livestock density data are for the year 2007, population density data are for the year 2017.

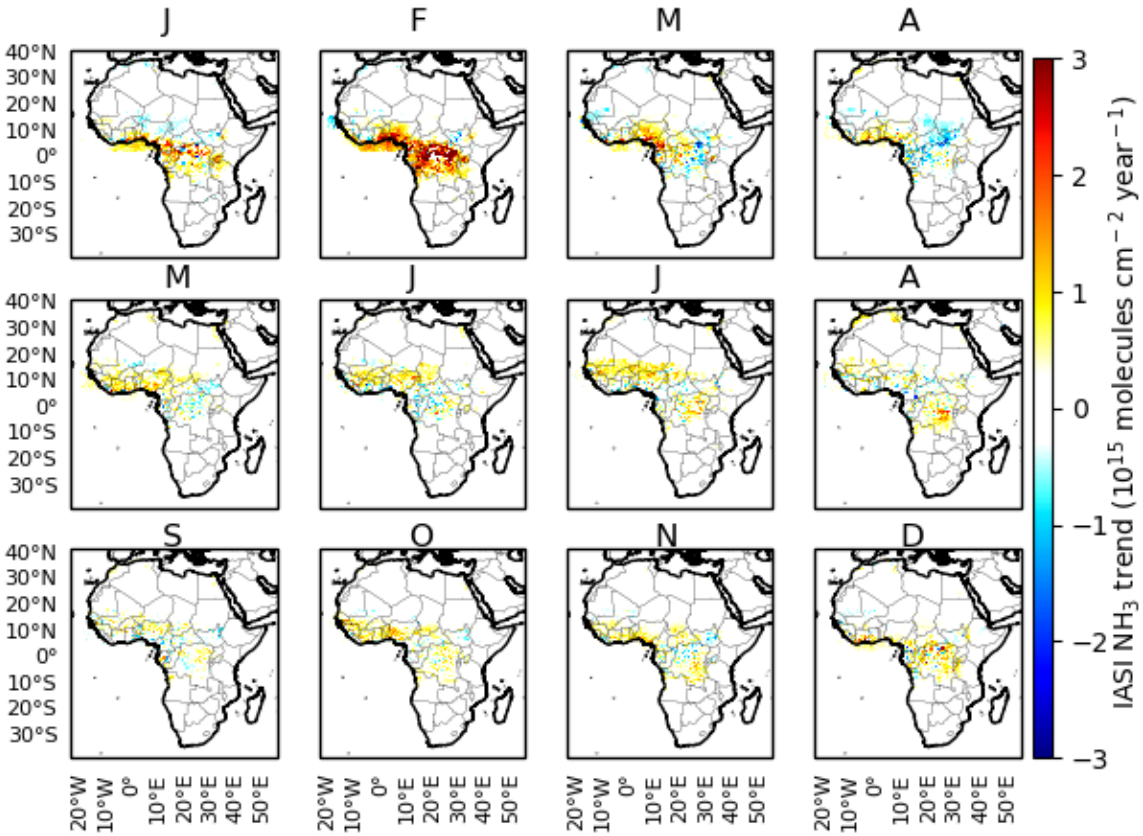


291

292 **Figure 3.** Change in mean monthly atmospheric $NH_3$ VCDs for the period 2008 through
293 2018. Grid cells where mean annual $NH_3$ VCDs for the entire period are under $5x10^{15}$
294 molecules $cm^{-2}$ are not displayed. Results significant at P=0.05 are presented in Figure S5.

295

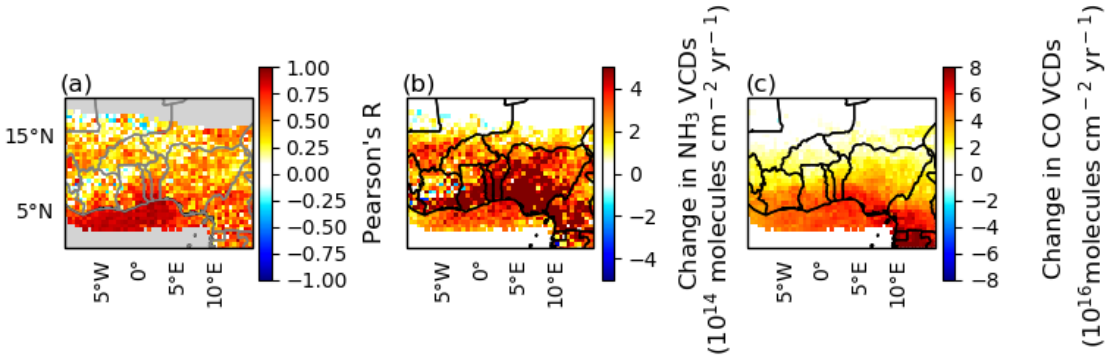


296

297

298 **Figure 4.** Correlation coefficient for the relationship between mean annual CO and
299 $NH_3$ VCDs (a), changes in $NH_3$ VCDs (b) and changes in CO VCDs (c) over 2008 through
300 2018 in West Africa. Grid cells where mean annual $NH_3$ VCDs for the entire period are
301 under $5x10^{15}$ molecules $cm^{-2}$ are not displayed. Results significant at P=0.05 for the entire
302 continent are presented in Figure S6.

303

304 **3.2 West Africa**

305 The increasing trend in $NH_3$ VCDs over West Africa are centered over Nigeria and
306 the southern coast, and to a lesser extent across parts of the wet savanna (Fig. 1b).
307 Increases in $NH_3$ VCDs tend to be higher in grid cells with higher population densities in
308 Nigeria and other parts of West Africa (Fig. 2b), suggesting a possible anthropogenic
309 influence. The spatial distribution of the mean annual $NH_3$ trend is overlapped by a
310 substantial increase in mean annual CO VCDs (Fig. 1b, 1d), pointing to a biomass burning
311 source, as is also the case in central Africa. Earlier studies have found substantial declines
312 in annual burned area across the north equatorial African biomass burning region as
313 detected by MODIS (Andela et al., 2017; Andela and van der Werf, 2014) and related
314 declines in $NO_2$ VCDs across the region (Hickman et al., 2021a), which would seem to stand
315 in contrast to the increasing CO and $NH_3$ trends observed here.
316 However, the annual decline in burned area and $NO_2$ VCDs is characterized by
317 heterogeneity when considering individual months. In West Africa, the dry season is
318 typically November to February or March. During the transition from the dry to rainy
319 season in February and March, $NO_2$ VCDs exhibit increasing rather than decreasing trends
320 in West Africa, though burned area patterns are not as clear when 2018 is included
321 (Hickman et al., 2021a; Fig. S2, S3). Although these increases in $NO_2$ VCDs are small in the
322 annual context, they occur at a time of year when biomass burning combustion is less
323 complete, potentially due to greater fuel moisture and declining fire radiative power
324 (Hickman et al., 2021a; Zheng et al., 2018). These conditions would lead to greater

emissions of less oxidized species such as CO and $NH_3$, rather than the more fully oxidized species such as $CO_2$ and $NO_2$ that dominate emissions during the peak of the biomass burning season (Fig. S2, S4). Indeed, our observations suggest that much of the increasing $NH_3$ trend occurs during this transitional period, with $NH_3$ VCDs increasing by roughly 6% $yr^{-1}$ for all of Nigeria during February and March (Fig. 3, S5; $p<0.01$). Variation in $NH_3$ VCDs are positively correlated with CO VCDs (Fig. 4a, S6), which are also increasing during this period (Fig. 4c, S4).

These correlations imply a biomass burning source for the increasing $NH_3$ VCDs in West Africa; although the burned area trends are not as clear, it is important to remember that MODIS undercounts burned area during this time of year by a factor of 3 to 6, and so would be less sensitive to trends (Ramo et al., 2021; Roteta et al., 2019). Although there is considerable gas flaring in Nigeria, gas flaring emissions have exhibited long-term negative trends (Doumbia et al., 2019). In addition, although $NO_2$ VCDs were found to decrease across the productive savannas of West Africa, regions of increasing $NO_2$ VCDs were observed over large parts of Nigeria, further suggesting that there may be increases—or at least smaller decreases—in biomass burning in the country (Hickman et al., 2021a). It is unlikely that changes in chemical sinks—specifically, the formation of nitrate aerosols in reactions with $NO_x$ or sulfate—are responsible for the increasing trend: the observed increase in $NO_2$ VCDs observed during February and March would be expected to lead to a shorter $NH_3$ lifetime and decreasing VCDs. In addition, emissions of $SO_2$ are relatively low in West Africa, with moderate emissions occurring in Nigeria, but neither emissions nor lifetime exhibit clear seasonal variation (Lee et al., 2011).

Small agricultural fires are likely an important contributor to the increasing $NH_3$ VCDs during the dry-to-rainy season transitional period—a period when agricultural fires are common in the region (Korontzi et al., 2006). There are large numbers of small fires that are not detected by MODIS during these months: as noted above, estimates of burned area during February, March, and April are revised upwards by roughly a factor of 3 to 6 over MODIS when small fires are included (Ramo et al., 2021; Roteta et al., 2019). Many of these small fires are likely related to agricultural field preparation prior to planting (Gbadegesin and Olusesi, 1994), which typically takes place in March or April (Vrieling et al., 2011; Yegbemey et al., 2014). An increase in fires during this transitional period is also

356 consistent with one of the primary mechanisms behind the overall decline in burned area:
357 roughly half of the decline is attributed to increased population density and the expansion
358 of agricultural area, which contributes to the anthropogenic suppression of larger fires
359 (Andela et al., 2017; Andela and van der Werf, 2014). This agricultural expansion,
360 however, can be expected to be accompanied by increases in small fires used for the
361 removal of stubble or harvest byproduct (Gbadegesin and Olusesi, 1994), leading to the
362 increased emissions during the rainy-to-dry season transition observed here.
363 Globally, agricultural emissions from fertilized soils and livestock excreta are the
364 largest source of $NH_3$ (Bauer et al., 2016), and Warner et al. (Warner et al., 2017) suggest
365 that national-scale changes in fertilizer use could explain the $NH_3$ trend over Nigeria.
366 However, as noted above, much of the increase in West Africa occurs prior to the start of
367 the planting season—before fertilizer is applied—and appears likely to be due to biomass
368 burning emissions instead, potentially related to field preparation. Fertilizer or manure
369 may make a contribution to the increasing trend later in the year, as $NH_3$ VCDs increase in
370 the wet savanna during May, June, and July (Fig. 3), though there are also significant
371 correlations between $NH_3$ and CO VCDs (Fig. 4), suggesting that biomass burning may
372 continue to play an important role. However, average N fertilizer use in West Africa is
373 universally under 40 kg N $ha^{-1}$ $yr^{-1}$, typically under 20 kg N $ha^{-1}$ $yr^{-1}$, and is under 10 kg N
374 $ha^{-1}$ $yr^{-1}$ in Nigeria—over an order of magnitude lower than rates in Europe, the United
375 States, and China (FAO, 2020). Although percentage changes in fertilizer use are
376 substantial, in absolute terms they represent increases of less than 2 kg N $ha^{-1}$ $yr^{-1}$, and
377 frequently less than 1 kg N $ha^{-1}$ $yr^{-1}$, a relatively small but perhaps not entirely trivial
378 perturbation to the N cycle: Between 2000 and 2007, total N deposition averaged 8.38 kg N
379 $ha^{-1}$ $yr^{-1}$ in wet savanna and 14.75 kg N $ha^{-1}$ $yr^{-1}$ in forest ecosystems based on surface
380 sampling sites (Galy-Lacaux and Delon, 2014), and biological N fixation in tropical and wet
381 savannas has been estimated as ranging from 16 to 44 kg N $ha^{-1}$ $yr^{-1}$ (Bustamante et al.,
382 2006). These estimates suggest that fertilizer increases may represent a 1 to 2% annual
383 increase in N inputs. But given the small magnitude of fertilizer applications, it appears
384 unlikely that changes in fertilizer use can explain the entirety of $NH_3$ increases during the
385 growing season. Our analyses do suggest that livestock may contribute to increasing $NH_3$
386 VCDs over the Sahel, from roughly 15 to 18N (Fig. 2a). However, many of these pixels are

387 also those where population density appears to be playing a role (Figure 2b) and where
388 correlations between $NH_3$ and CO VCDs are present during the transition from the dry to
389 rainy season (Fig. S7), which may reflect a contribution from agricultural fires.
390

391 **3.3. South Sudan**

392 The most notable declining trend in $NH_3$ VCDs occurs in South Sudan over the Sudd
393 wetlands at a rate of over 2% $yr^{-1}$ (Fig. 1b; p=0.20). It appears that this decline is related to
394 interannual variation in the flooded extent of the Sudd, a vast wetland that connects the
395 White and Blue Nile tributaries. Seasonal variation of inflow to the Sudd leads to variation
396 in flooded extent: an area of roughly 15,000 $km^2$ is permanently flooded, and another
397 roughly 15,000 $km^2$ is temporarily flooded each year, with considerable interannual
398 variation in the total flooded area (Di Vittorio and Georgakakos, 2018). Among other
399 factors, drying soils should increase production and emissions of $NH_3$ from soils, as Eq. 1 is
400 shifted to the right (Clarisse et al., 2019). Earlier work evaluating an $NH_3$ hotspot over Lake
401 Natron in Tanzania found that the drying of seasonally flooded soils leads to large
402 emissions of $NH_3$: As the waters of Lake Natron recede during the dry season each year
403 and the surrounding mud flats dry out, $NH_3$ VCDs increase rapidly, with hotspots appearing
404 over the mudflats (Clarisse et al., 2019). These elevated VCDs are attributed to multiple
405 possible factors, including the effects of drying on concentrations of $NH_3$ in solution (which
406 increases the concentration gradient with the atmosphere), reduced biological uptake of
407 $NH_3$, convective transport of dissolved $NH_3$ from depth to the soil surface, and increased
408 mineralization of labile organic matter (Clarisse et al., 2019).

409 We find the same clear seasonal relationship between wetland flooded extent and
410 $NH_3$ concentrations over the Sudd—VCDs increase as waters recede from the temporarily
411 flooded area, leading to annual maxima from February through May (Fig. 5a; bounding box
412 of 29E to 31.5E and 6N to 9.9N). Like the entire country, seasonal variation in $NH_3$ VCDs
413 over the Sudd follow variation in surface temperature, but $NH_3$ concentrations over the
414 Sudd are substantially elevated compared to surrounding regions during this time of year
415 but not others, suggesting that a mechanism in addition to temperature is contributing to

the elevated emissions in the Sudd during February through May, a period that spans the end of the dry season and start of the rainy season (Fig. S8). This conclusion is supported by an analysis of interannual variation of VCDs during the February through May period: Interannual variation in $NH_3$ VCDs is largely decoupled from variation in temperature, but $NH_3$ VCDs appear to vary inversely with the amount of area that dries out each year (Fig. 5b). Over the period for which flooded extent data are currently available for the Sudd, the minimum flooded extent tends to increase—that is, less area dries out each year—resulting in an overall decline in $NH_3$ VCDs. Linear regression reveals that this change in flooded extent explains a large proportion of the annual variation in $NH_3$ in the Sudd bounding box (r=-0.64, p=0.046), as well as for the country as a whole (r=-0.60, p=0.065). These analyses strongly suggest that the declining trend in $NH_3$ over the Sudd is a direct result of an overall increase in the minimum flooded extent over the observation period.

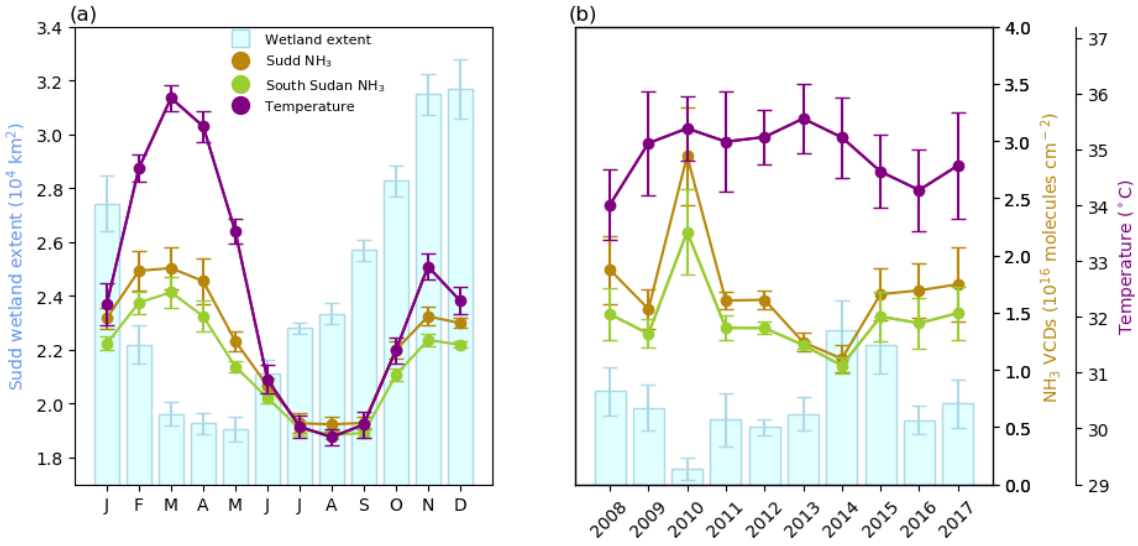


**Figure 5.** Mean (a) monthly and (b) February through May annual mean flooded extent of the Sudd, surface temperatures over South Sudan, and $NH_3$ VCDs over the Sudd and the entirety of South Sudan for the period 2008 through 2017.

435
436

437 It is possible that conflict in South Sudan could contribute to the decline in $NH_3$
438 VCDs. In 2013, a civil conflict emerged in South Sudan that was ultimately responsible for
439 the displacement of millions of people (Global Internal Displacement Monitoring Centre,
440 2020; World Bank, 2019) and the disruption of livestock migration patterns (Idris, 2018).
441 However, these disruptions appeared only after the onset of the long-term change in $NH_3$,
442 and appear unlikely to make an important contribution to the observed interannual
443 variation (SI Text, Fig. S9, S10).

444 It is unlikely that changes in chemical sinks are responsible for the decline in $NH_3$
445 VCDs. VCDs of tropospheric $NO_2$ are also decreasing in the region (Fig. S11), which is
446 suggestive of less formation of particulate-phase ammonium rather than more.
447 Anthropogenic $SO_2$ emissions in Africa in general and South Sudan in particular are very
448 low (European Commission Joint Research Centre (JRC)/Netherlands Environmental
449 Assessment Agency (PBL), 2016), and would not be expected to be emitted from the Sudd;
450 more generally, the clear spatial association between the $NH_3$ trend and the Sudd (Fig. 1,
451 Fig. S12) is strongly suggestive of changes in emissions rather than atmospheric processes
452 being responsible for the trend.

453

454 **3.4 Lake Victoria Basin region**

455 The Lake Victoria Basin and its surroundings—an area including elevated mean $NH_3$
456 VCDs—exhibit an increasing $NH_3$ trend (Fig. 1b, Fig. 7, Fig. S13), which appears to be the
457 result of increasing agricultural activity in the area. The region includes a high and
458 increasing density of agricultural land (Fig. 1h, Fig. 2d, Fig. S14), and these increases in
459 cropped area are positively correlated with increases in $NH_3$ VCDs across much of the
460 region (Fig. 2c). The northern and southern halves of the Lake Victoria region—which
461 straddles the equator—have distinct growing seasons: in the north, the season generally

starts in April, whereas in the south, it starts in November or December (Vrieling et al., 2011). Some of the long-term trend reflects this seasonality, with increases in the north and south occurring during their respective growing seasons (Fig. 3, Fig. S15). Fertilizer use in the Lake Victoria region is low: national averages range from about 1 to 3 kg nutrients $ha^{-1}$ $yr^{-1}$ in Uganda to about 35 to 40 kg nutrients $ha^{-1}$ $yr^{-1}$ in Kenya (Elrys et al., 2019; World Bank, 2019); to put these numbers in context, Organization for Economic Cooperation and Development (OECD) countries use about 135-140 kg nutrients $ha^{-1}$ $yr^{-1}$ (World Bank, 2019). Although rates of fertilizer use have increased by substantial proportions, the absolute amount of increase is relatively small, typically roughly 1 to 10 kg nutrients $decade^{-1}$. Unlike in West Africa, however, interannual variation in burned area (Fig. 7, S16) does not exhibit a clear relationship with changes in $NH_3$ VCDs. Consequently, we expect that both the expansion and intensification of agriculture in the region contribute to the increasing $NH_3$ VCDs.

We note that there is a negative correlation between cropland area and $NH_3$ VCDs in Uganda, north of Lake Victoria (Figure 7b). We expect this is a consequence of the extremely low fertilizer use in Uganda (Masso et al., 2017) , which leads to depletion of soil N—and thus substrate for ammonia volatilization—over time (Cobo et al., 2010).

We also note that there is an apparent increase in $NH_3$ VCDs over the lake itself. It is important to note that differences in conditions over the lake and adjacent land cover—e.g., emissivity, thermal contrast, etc.—contribute to substantial differences in mean retrieved $NH_3$ VCDs over the lake relative to the surrounding land surface. Both monthly and interannual variation in $NH_3$ VCDs over Lake Victoria correspond closely to variation in $NH_3$ VCDs over the surrounding land surface (Figure S17, S18), suggesting that the trend over the lake results from transport of $NH_3$ emitted from the surrounding land surface.

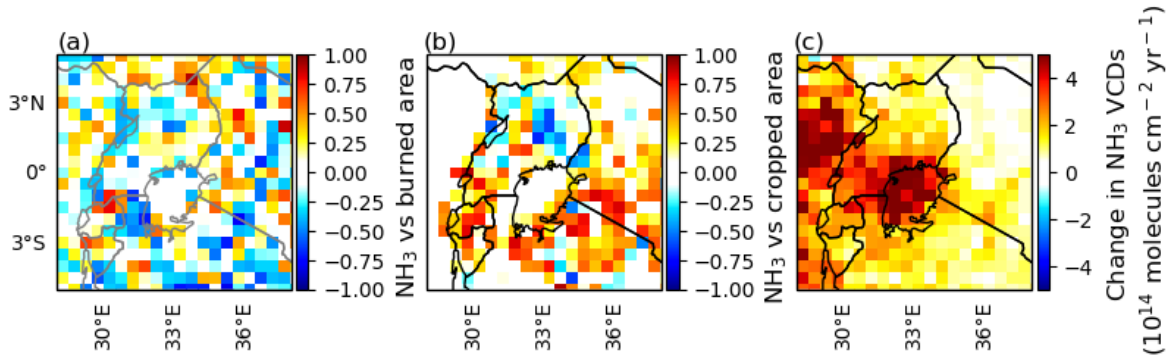


**Figure 7. Changes in $NH_3$ VCDs and their relationship with burned area and cropped area** over the Lake Victoria region for the 2008 through 2018 period. (a) Correlation coefficients for the relationship between $NH_3$ VCDs and burned area. (b) Correlation coefficients for the relationship between $NH_3$ VCDs and cropped area, including mosaics of crops and natural vegetation cover. (c) Changes in $NH_3$ VCDs.

### 3.5 National-scale relationships

Examining relationships at a national scale can provide insight into relationships between changes in agricultural or biomass burning and changes in atmospheric $NH_3$ VCDs at larger scales. When grouping countries into three bins based on their annual percentage changes in $NH_3$ VCDs, there is some evidence for a broad relationship between livestock and $NH_3$ VCDs at the national scale (Fig. 8). The rate of change in national-scale $NH_3$ VCDs varies significantly among bins ($p<0.001$; rank transformed, though note that residuals may still deviate from normality). The annual percentage changes in livestock in TLUs vary significantly by bin ($p=0.042$; rank transformed), with the middle bin higher than the bottom bin ($p=0.1$) and the high bin higher than the bottom bin ($p=0.06$). Annual percentage changes in fertilizer N ($p=0.58$) and crop production ($p=0.62$; rank transformed) did not vary by bin.

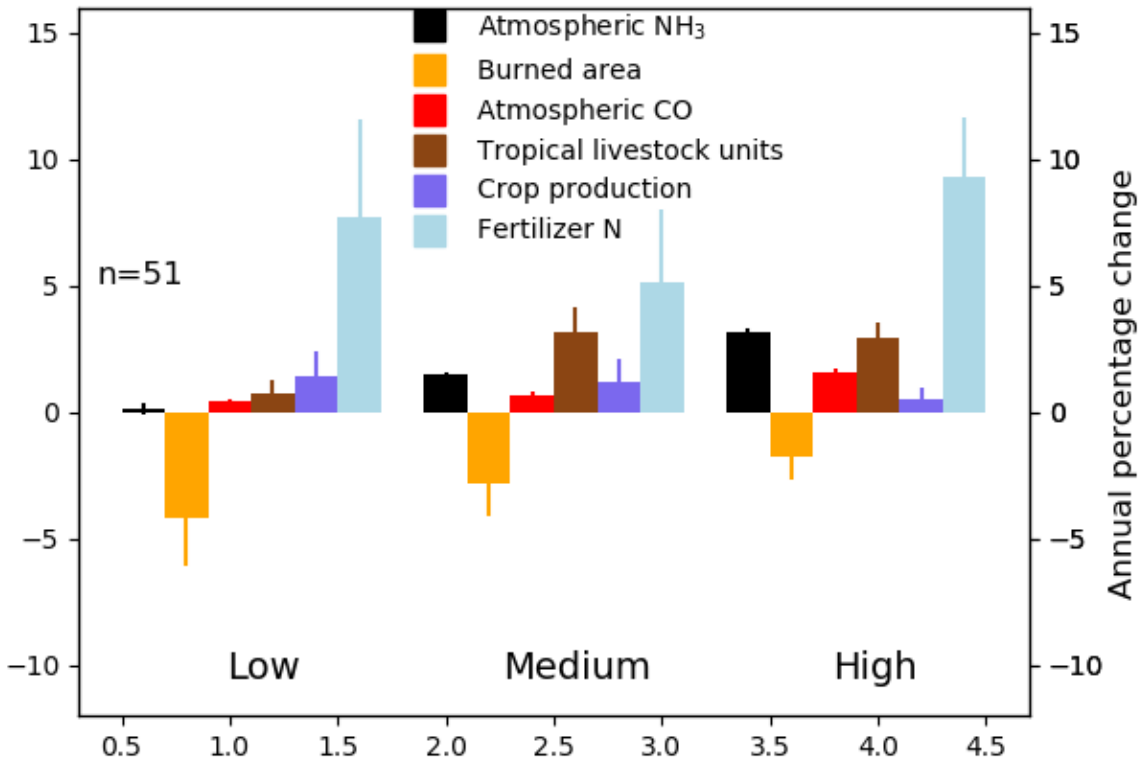


**Figure 8.** Annual percentage changes in national mean annual $NH_3$ VCDs, burned area, CO VCDs, livestock, crop yield, and fertilizer N use for African countries with low, medium, or high rates of $NH_3$ VCD change. Error bars represent the standard error of the mean. See Table S1 for the list of countries in each bin and Fig. S19 for an expanded set of variables.

Instead of a direct agricultural relationship with changes in $NH_3$ VCDs, there is the possibility that changes in biomass burning are associated with changes in $NH_3$ VCDs. Although the differences in the annual percentage change in burned area were not significant among bins ($p=0.54$; rank transformed), the overall pattern is consistent with earlier results finding that a reduction in burned area across the northern biomass burning region was associated in part with the expansion of agriculture and presumed anthropogenic suppression of fire (Andela et al., 2017; Andela and van der Werf, 2014). However, burned area as measured by MODIS is likely an imperfect predictor for $NH_3$

emissions—as noted previously, MODIS underestimates burned area by a factor of 3 to 6 during shoulder seasons (Roteta et al., 2019), which is when fires are expected to emit more reduced species such as $NH_3$ (Zheng et al., 2018). In contrast to burned area, the annual change in column densities of CO—which tends to be co-emitted with $NH_3$ from fires—differed significantly among bins ($p<0.001$; rank transformed) and was significantly higher in the high bin than in the low or medium bins ($p<0.001$, post-hoc tests). The higher annual CO changes in the high bin could related to larger anthropogenic fossil fuel emissions, but we see no difference among bins in growth rates of $CO_2$ emissions ($p=0.48$; Figure S19); such a difference would be expected if differences in economic development were responsible for the CO differences. These results leave open the possibility that changes in either biofuel emissions or biomass burning emissions—perhaps from smaller fires not observed in the MODIS burned area product—may be primarily responsible for the difference in CO between bins, and may be contributing to the differences in $NH_3$ between bins. Changes in $NO_2$ VCDs and $SO_2$ concentrations can affect the lifetime of $NH_3$ (the latter by changing $SO_4$ concentrations), but do not appear to make an important contribution to the observed trends in $NH_3$ VCDs among bins (Fig. S19, SI text). Temperature, likewise, does not appear to play an important role (SI text).

## 4. Conclusion

Using IASI, we have observed both increases and decreases in atmospheric $NH_3$ VCDs in different regions in Africa between 2008 and 2018, with different factors affecting trends in different regions.

We observed increases in $NH_3$ VCDs in West Africa, which earlier work had concluded was likely related to increased fertilizer use. Fertilizer is not typically applied in West Africa until the start of the growing season—often April—but we find that much of the $NH_3$ increase occurs during February and March, suggesting that increasing fertilizer use is unlikely to provide a complete explanation for the $NH_3$ trend. Agriculture may nevertheless play a role, with enhanced burned area and especially CO concentrations in February suggestive of increased burning of crop stubble in preparation for planting during this time of year. Fires in this region tend to emit a greater proportion of less oxidized

551 species such as $NH_3$ at the end of the dry season, consistent with a biomass burning source
552 for the increasing $NH_3$ VCDs.
553 Decreases in $NH_3$ VCDs were largest in South Sudan, especially over the Sudd
554 wetland, where $NH_3$ VCDs vary seasonally with the extent of area flooded. As the
555 temporarily flooded areas of the Sudd dry out each year, $NH_3$ VCDs increase as reduction in
556 soil moisture drives increased production and volatilization of $NH_3$. The area of the Sudd
557 that is flooded each year varies, and from 2008 until 2015, the area that remains flooded
558 during the dry season generally increased, producing a positive overall trend for the period
559 of 2008 through 2017. This increase in the dry season flooded area drove a decrease in
560 $NH_3$ VCDs: with less soil drying out, the seasonal maxima in $NH_3$ VCDs were lower.
561 Although it is possible that conflict in South Sudan could contribute to changes in $NH_3$
562 VCDs, the timing and distribution of conflict events and human displacement suggest that
563 other factors are likely more important.
564 Modest increases in $NH_3$ VCDs were observed in the Lake Victoria region. This
565 region has experienced increases in agricultural area during the IASI observation period,
566 and these changes explained a large proportion of the variation in $NH_3$ VCDs across large
567 patches of the region, where biomass burning could not. We expect that both expansion
568 and intensification of agriculture in this region could contribute to the positive $NH_3$ trend.
569 Considering national-scale statistics, comparisons between equally sized bins of 17
570 countries each suggested that changes in biomass burning emissions and livestock
571 emissions could contribute to differences in $NH_3$ VCDs among countries, but variables
572 related to cropped agriculture such as cropped area or fertilizer N use did not appear to be
573 important factors at this scale. This may be because although fertilizer use has been
574 increasing in sub-Saharan Africa, it remains extremely low relative to other continents, and
575 relative to the levels needed to attain food security. Average fertilizer use in most
576 countries in the region is under 20 kg N $ha^{-1}$ $yr^{-1}$, and sometimes less than 5 kg N $ha^{-1}$ $yr^{-1}$.
577 Although recommended fertilizer rates are lower in most African countries than in the U.S.
578 or Europe, increasing N inputs to 50 or 100 kg N $ha^{-1}$ $yr^{-1}$ would represent a major
579 perturbation to the regional N cycle, and potentially a large new source of $NH_3$ to the
580 atmosphere. West Africa is already a global $NH_3$ hotspot (Van Damme et al., 2018),
581 suggesting that encouraging policies that can help to limit $NH_3$ emissions during the early

582 stages of agricultural intensification in Africa may help mitigate potential impacts on the
583 atmosphere. Fortunately, agricultural practices such as sub-surface application of
584 fertilizer, which is already being promoted to smallholder farmers, can serve to both limit
585 $NH_3$ emissions also help to increase crop yields.
586 These past and anticipated future trends also make the case for expanding capacity
587 for atmospheric monitoring in sub-Saharan Africa. Although long-term monitoring
588 networks have been established in West Africa (Adon et al., 2010; Ossohou et al., 2019) and
589 South Africa (Conradie et al., 2016) as part of the INDAAF network, it is mainly focused on
590 deposition and the spatio-temporal resolution of surface measurements is very coarse
591 when compared to the data available in other parts of the world, which will limit our ability
592 to understand how agricultural and socio-economic development in Africa affect the
593 atmosphere. Satellite observations can help to bridge some of these data gaps, but have
594 their own spatio-temporal limitations, and would further benefit from additional high-
595 quality surface observations for evaluation of retrieval products.
596

597 **Data availability:** All data used in this study are available from public sources, with the
598 exception of Sudd wetland extent, which is available by request from Courtney Di Vittorio. The
599 IASI $NH_3$ and CO data are available from The IASI https://iasi.aeris-data.fr. The NOAA Global
600 Surface Temperature Dataset is available at https://data.nodc.noaa.gov/cgi-
601 bin/iso?id=gov.noaa.ncdc:C01585. MODIS burned area data are available from
602 https://www.globalfiredata.org/data.html. MODIS agricultural area are available at
603 https://lpdaac.usgs.gov/products/mcd12c1v006/. TRMM 3B42 precipitation data are available
604 from https://pmm.nasa.gov/data-access/downloads/trmm. The Gridded Livestock of the World
605 data are available from https://livestock.geo-wiki.org/home-2/. Population density data for 2017
606 are available at https://landscan.ornl.gov/downloads/2017. FAO national crop production and
607 fertilizer N data are available at http://www.fao.org/faostat/en/. Data on conflict events from
608 ACLED are available at https://acleddata.com/#/dashboard. World Bank national statistics
609 on refugees and internally displaced people are available at https://data.worldbank.org.

610

**Author Contribution:** J.E.H. designed the study, conducted the analysis, and wrote the paper. NA, ED, CD, MO, CG-L, KT, and SEB contributed to study design and edited the paper. LC, P-FC, and MVD developed the original IASI trace gas retrievals and edited the paper.

The authors declare that they have no conflict of interest.

**Acknowledgements: J.E.H.'s** research was supported by an appointment to the NASA Postdoctoral Program at the NASA Goddard Institute for Space Studies administered by Universities Space Research Association under contract with NASA.

## References

van der A, R. J., Eskes, H. J., Boersma, K. F., van Noije, T. P. C., Van Roozendael, M., De Smedt, I., Peters, D. H. M. U. and Meijer, E. W.: Trends, seasonal variability and dominant NOx source derived from a ten year record of NO2 measured from space, J. Geophys. Res. Atmos., 113(4), D04302, doi:10.1029/2007JD009021, 2008.

Adon, M., Galy-Lacaux, C., Yoboué, V., Delon, C., Lacaux, J. P., Castera, P., Gardrat, E., Pienaar, J., Al Ourabi, H., Laouali, D., Diop, B., Sigha-Nkamdjou, L., Akpo, a., Tathy, J. P., Lavenu, F. and Mougin, E.: Long term measurements of sulfur dioxide, nitrogen dioxide, ammonia, nitric acid and ozone in Africa using passive samplers, Atmos. Chem. Phys., 10(15), 7467–7487, doi:10.5194/acp-10-7467-2010, 2010.

AGRA: AGRA in 2008: Building on the New Momentum in African Agriculture., 2009.

Andela, N. and van der Werf, G. R.: Recent trends in African fires driven by cropland expansion and El Niño to la Niña transition, Nat. Clim. Chang., 4(9), 791–795, doi:10.1038/nclimate2313, 2014.

Andela, N., Morton, D. C., Giglio, L., Chen, Y., Van Der Werf, G. R., Kasibhatla, P. S., DeFries, R. S., Collatz, G. J., Hantson, S., Kloster, S., Bachelet, D., Forrest, M., Lasslop, G., Li, F., Mangeon, S., Melton, J. R., Yue, C. and Randerson, J. T.: A human-driven decline in global burned area, Science (80-. )., 356(6345), 1356–1362, doi:10.1126/science.aal4108, 2017.

Anker, H. T., Baaner, L., Backes, C., Keessen, A. and Möckel, S.: Comparison of ammonia regulation in Germany , the Netherlands and Denmark – legal framework, Copenhagen.,

641 2018.
642 Bauer, S. E., Tsigaridis, K. and Miller, R.: Significant atmospheric aerosol pollution caused by
643 world food cultivation, Geophys. Res. Lett., 43(10), 5394–5400,
644 doi:10.1002/2016GL068354, 2016.
645 Behera, S. N., Sharma, M., Aneja, V. P. and Balasubramanian, R.: Ammonia in the
646 atmosphere: A review on emission sources, atmospheric chemistry and deposition on
647 terrestrial bodies, Environ. Sci. Pollut. Res., 20(11), 8092–8131, doi:10.1007/s11356-013-
648 2051-9, 2013.
649 Bouwman, A. F., Lee, D. S., Asman, W. A. H., Dentener, F. J., Van Der Hoek, K. W. and Olivier, J.
650 G. J.: A global high-resolution emission inventory for ammonia, Global Biogeochem. Cycles,
651 11(4), 561–587, 1997.
652 Bustamante, M. M. C., Medina, E., Asner, G. P., Nardoto, G. B. and Garcia-Montiel, D. C.:
653 Nitrogen cycling in tropical and temperate savannas, Biogeochemistry, 79(1–2), 209–237,
654 doi:10.1007/s10533-006-9006-x, 2006.
655 Cahoon, D. R., Stocks, B. J., Levine, J. S., Cofer, W. R. and O'Neill, K. P.: Seasonal distribution of
656 African savanna fires, Nature, 359(6398), 812–815, doi:10.1038/359812a0, 1992.
657 Chen, L.-W. A., Verburg, P., Shackelford, A., Zhu, D., Susfalk, R., Chow, J. C. and Watson, J. G.:
658 Moisture effects on carbon and nitrogen emission from burning of wildland biomass,
659 Atmos. Chem. Phys., 10(14), 6617–6625, doi:10.5194/acp-10-6617-2010, 2010.
660 Chilonda, P. and Otte, J.: Indicators to monitor trends in livestock production at national,
661 regional and international levels, Livest. Res. Rural Dev., 18(8), 1–12, 2006.
662 Clarisse, L., Clerbaux, C., Dentener, F., Hurtmans, D. and Coheur, P. F.: Global ammonia
663 distribution derived from infrared satellite observations, Nat. Geosci., 2(7), 479–483,
664 doi:10.1038/ngeo551, 2009.
665 Clarisse, L., Van Damme, M., Gardner, W., Coheur, P.-F., Clerbaux, C., Whitburn, S., Hadji-
666 Lazaro, J. and Hurtmans, D.: Atmospheric ammonia (NH3) emanations from Lake Natron's
667 saline mudflats, Sci. Rep., 9, 4441, doi:10.1038/s41598-019-39935-3, 2019.
668 Cobo, J. G., Dercon, G. and Cadisch, G.: Nutrient balances in African land use systems across
669 different spatial scales: A review of approaches, challenges and progress, Agric. Ecosyst.
670 Environ., 136(1–2), 1–15, doi:10.1016/j.agee.2009.11.006, 2010.
671 Conradie, E. H., Van Zyl, P. G., Pienaar, J. J., Beukes, J. P., Galy-Lacaux, C., Venter, A. D. and

672 Mkhatshwa, G. V.: The chemical composition and fluxes of atmospheric wet deposition at
673 four sites in South Africa, Atmos. Environ., 146, 113–131,
674 doi:10.1016/j.atmosenv.2016.07.033, 2016.
675 Van Damme, M., Wichink Kruit, R. J., Schaap, M., Clarisse, L., Clerbaux, C., Coheur, P. F.,
676 Dammers, E., Dolman, A. J. and Erisman, J. W.: Evaluating 4 years of atmospheric ammonia
677 (NH3) over Europe using IASI satellite observations and LOTOS-EUROS model results, J.
678 Geophys. Res., 119(15), 9549–9566, doi:10.1002/2014JD021911, 2014a.
679 Van Damme, M., Clarisse, L., Heald, C. L., Hurtmans, D., Ngadi, Y., Clerbaux, C., Dolman, A. J.,
680 Erisman, J. W. and Coheur, P. F.: Global distributions, time series and error characterization
681 of atmospheric ammonia NH3 from IASI satellite observations, Atmos. Chem. Phys., 14(6),
682 2905–2922, doi:10.5194/acp-14-2905-2014, 2014b.
683 Van Damme, M., Clarisse, L., Dammers, E., Liu, X., Nowak, J. B., Clerbaux, C., Flechard, C. R.,
684 Galy-Lacaux, C., Xu, W., Neuman, J. A., Tang, Y. S., Sutton, M. A., Erisman, J. W. and Coheur, P.
685 F.: Towards validation of ammonia (NH3) measurements from the IASI satellite, Atmos.
686 Meas. Tech., 8(3), 1575–1591, doi:10.5194/amt-8-1575-2015, 2015.
687 Van Damme, M., Whitburn, S., Clarisse, L., Clerbaux, C., Hurtmans, D. and Coheur, P. F.:
688 Version 2 of the IASI NH3 neural network retrieval algorithm: Near-real-time and
689 reanalysed datasets, Atmos. Meas. Tech., 10(12), 4905–4914, doi:10.5194/amt-10-4905-
690 2017, 2017.
691 Van Damme, M., Clarisse, L., Whitburn, S., Hadji-Lazaro, J., Hurtmans, D., Clerbaux, C. and
692 Coheur, P.: Industrial and agricultural ammonia point sources exposed, Nature, 564, 99–
693 103, 2018.
694 Van Damme, M., Clarisse, L., Franco, B., Sutton, M. A., Erisman, J. W., Wichink Kruit, R., van
695 Zanten, M., Whitburn, S., Hadji-Lazaro, J., Hurtmans, D., Clerbaux, C. and Coheur, P.-F.:
696 Global, regional and national trends of atmospheric ammonia derived from a decadal
697 (2008-2018) satellite record, Environ. Res. Lett., 2021.
698 Dammers, E., Palm, M., Van Damme, M., Vigouroux, C., Smale, D., Conway, S., Toon, G. C.,
699 Jones, N., Nussbaumer, E., Warneke, T., Petri, C., Clarisse, L., Clerbaux, C., Hermans, C.,
700 Lutsch, E., Strong, K., Hannigan, J. W., Nakajima, H., Morino, I., Herrera, B., Stremme, W.,
701 Grutter, M., Schaap, M., Kruit, R. J. W., Notholt, J., Coheur, P. F. and Erisman, J. W.: An
702 evaluation of IASI-NH3 with ground-based Fourier transform infrared spectroscopy

703 measurements, Atmos. Chem. Phys., 16(16), 10351–10368, doi:10.5194/acp-16-10351-
704 2016, 2016.
705 Denier Van Der Gon, H. and Bleeker, A.: Indirect N2O emission due to atmospheric N
706 deposition for the Netherlands, Atmos. Environ., 39(32), 5827–5838,
707 doi:10.1016/j.atmosenv.2005.06.019, 2005.
708 Dobson, J. E., Bright, E. A., Coleman, P. R., Durfee, R. C. and Worley, B. A.: A global population
709 database for estimating populations at risk, Photogramm. Eng. Remote Sens., 66(7), 849–
710 857 [online] Available from: In Book..., 2000.
711 Doumbia, E. H. T., Liousse, C., Keita, S., Granier, L., Granier, C., Elvidge, C. D., Elguindi, N. and
712 Law, K.: Flaring emissions in Africa: Distribution, evolution and comparison with current
713 inventories, Atmos. Environ., 199(November 2018), 423–434,
714 doi:10.1016/j.atmosenv.2018.11.006, 2019.
715 Elrys, A. S., Abdel-Fattah, M. K., Raza, S., Chen, Z. and Zhou, J.: Spatial trends in the nitrogen
716 budget of the African agro-food system over the past five decades, Environ. Res. Lett.,
717 14(12), doi:10.1088/1748-9326/ab5d9e, 2019.
718 European Commission Joint Research Centre (JRC)/Netherlands Environmental
719 Assessment Agency (PBL): Emission Database for Global Atmospheric Research (EDGAR),
720 release version 4.3.1, 2016.
721 Fan, Y. and van den Dool, H.: A global monthly land surface air temperature analysis for
722 1948-present, J. Geophys. Res. Atmos., 113(1), D01103, doi:10.1029/2007JD008470, 2008.
723 FAO: FAO Statistics Database, FAOSTAT Stat. Database [online] Available from:
724 http://www.fao.org/faostat/en/ (Accessed 1 January 2019), 2020.
725 Friedl, M. A., McIver, D. K., Hodges, J. C. F., Zhang, X. Y., Muchoney, D., Strahler, A. H.,
726 Woodcock, C. E., Gopal, S., Schneider, A., Cooper, A., Baccini, A., Gao, F. and Schaaf, C.: Global
727 land cover mapping from MODIS: Algorithms and early results, Remote Sens. Environ.,
728 83(1–2), 287–302, doi:10.1016/S0034-4257(02)00078-0, 2002.
729 Galy-Lacaux, C. and Delon, C.: Nitrogen emission and deposition budget in West and Central
730 Africa, Environ. Res. Lett., 9(12), doi:10.1088/1748-9326/9/12/125002, 2014.
731 Gbadegesin, A. and Olusesi, B. B.: Effects of land clearing methods on soil physical and
732 hydrological properties in southwestern Nigeria, Environmentalist, 14(4), 297–303
733 [online] Available from: http://www.scopus.com/inward/record.url?eid=2-s2.0-

0022858519&partnerID=40&md5=3051b1dd91ff2990e37fe7466872923e, 1994.
George, M., Clerbaux, C., Hurtmans, D., Turquety, S., Coheur, P. F., Pommier, M., Hadji-Lazaro, J., Edwards, D. P., Worden, H., Luo, M., Rinsland, C. and McMillan, W.: Carbon monoxide distributions from the IASI/METOP mission: Evaluation with other space-borne remote sensors, Atmos. Chem. Phys., 9(21), 8317–8330, doi:10.5194/acp-9-8317-2009, 2009.
Giglio, L., Boschetti, L., Roy, D. P., Humber, M. L. and Justice, C. O.: The Collection 6 MODIS burned area mapping algorithm and product, Remote Sens. Environ., 217, 72–85, doi:10.1016/j.rse.2018.08.005, 2018.
Global Internal Displacement Monitoring Centre: Global Internal Displacement Database, [online] Available from: https://www.internal-displacement.org/database/displacement-data, 2020.
Goode, J. G., Yokelson, R. J., Susott, R. A. and Ward, D. E.: Trace gas emissions from laboratory biomass fires measured by open-path Fourier transform infrared spectroscopy:, J. Chem. Inf. Model., 104(D17), 21237–21245, 1999.
Guo, X., Clarisse, L., Wang, R., Van Damme, M., Whitburn, S., Coheur, P., Clerbaux, C., Franco, B., Pan, D., Golston, L. M., Wendt, L., Sun, K., Tao, L., Miller, D., Mikoviny, T., Müller, M., Wisthaler, A., Tevlin, A. G., Murphy, J. G., Nowak, J. B., Roscioli, J. R., Volkamer, R., Kille, N., Neuman, J. A., Eilerman, S. J., Crawford, J. H., Yacovitch, T. I., Barrick, J. D., Scarino, A. J. and Zondlo, M. A.: Validation of IASI satellite ammonia observations at the pixel scale using in-situ vertical profiles, J. Geophys. Res. Atmos., 126, e2020JD033475, doi:10.1029/2020jd033475, 2021.
Hazell, P. and Wood, S.: Drivers of change in global agriculture., Philos. Trans. R. Soc. Lond. B. Biol. Sci., 363(1491), 495–515, doi:10.1098/rstb.2007.2166, 2008.
Hickman, J. E., Dammers, E., Galy-Lacaux, C. and Van Der Werf, G. R.: Satellite evidence of substantial rain-induced soil emissions of ammonia across the Sahel, Atmos. Chem. Phys., 18(22), 16713–16727, doi:10.5194/acp-18-16713-2018, 2018.
Hickman, J. E., Andela, N., Tsigaridis, K., Galy-Lacaux, C., Ossohou, M. and Bauer, S. E.: Reductions in NO 2 burden over north equatorial Africa from decline in biomass burning in spite of growing fossil fuel use, 2005 to 2017 , Proc. Natl. Acad. Sci., 118(7), e2002579118, doi:10.1073/pnas.2002579118, 2021a.

765 Hickman, J. E., Dammers, E., Galy-Lacaux, C., Ossohou, M. and Bauer, S. E.: Continental and
766 ecoregion-specific drivers of atmospheric NO2 and NH3 seasonality over Africa revealed by
767 satellite observations, Global Biogeochem. Cycles, 35, e2020GB006916,
768 doi:10.1029/2020GB006916, 2021b.
769 Huffman, G. J., Adler, R. F., Bolvin, D. T., Gu, G., Nelkin, E. J., Bowman, K. P., Hong, Y., Stocker,
770 E. F. and Wolff, D. B.: The TRMM Multisatellite Precipitation Analysis (TMPA): Quasi-Global,
771 Multiyear, Combined-Sensor Precipitation Estimates at Fine Scales, J. Hydrometeorol., 8(1),
772 38–55, doi:10.1175/jhm560.1, 2007.
773 Hurtmans, D., Coheur, P. F., Wespes, C., Clarisse, L., Scharf, O., Clerbaux, C., Hadji-Lazaro, J.,
774 George, M. and Turquety, S.: FORLI radiative transfer and retrieval code for IASI, J. Quant.
775 Spectrosc. Radiat. Transf., 113(11), 1391–1408, doi:10.1016/j.jqsrt.2012.02.036, 2012.
776 Idris, I.: Livestock and conflict in South Sudan - K4D Helpdesk Report 484, Brighton.
777 [online] Available from:
778 https://assets.publishing.service.gov.uk/media/5c6abdec40f0b61a22792fd5/484__Livest
779 ock_and_Conflict_in_South_Sudan.pdf, 2018.
780 Kanter, D. R.: Nitrogen pollution: a key building block for addressing climate change, Clim.
781 Change, 147(1–2), 11–21, doi:10.1007/s10584-017-2126-6, 2018.
782 Kerzenmacher, T., Dils, B., Kumps, N., Blumenstock, T., Clerbaux, C., Coheur, P. F., Demoulin,
783 P., García, O., George, M., Griffith, D. W. T., Hase, F., Hadji-Lazaro, J., Hurtmans, D., Jones, N.,
784 Mahieu, E., Notholt, J., Paton-Walsh, C., Raffalski, U., Ridder, T., Schneider, M., Servais, C. and
785 De Mazière, M.: Validation of IASI FORLI carbon monoxide retrievals using FTIR data from
786 NDACC, Atmos. Meas. Tech., 5(11), 2751–2761, doi:10.5194/amt-5-2751-2012, 2012.
787 Korontzi, S., McCarty, J., Loboda, T., Kumar, S. and Justice, C.: Global distribution of
788 agricultural fires in croplands from 3 years of Moderate Resolution Imaging
789 Spectroradiometer (MODIS) data, Global Biogeochem. Cycles, 20(2), GB2021,
790 doi:10.1029/2005GB002529, 2006.
791 Krupa, S. V.: Effects of atmospheric ammonia (NH3) on terrestrial vegetation: A review,
792 Environ. Pollut., 124(2), 179–221, doi:10.1016/S0269-7491(02)00434-7, 2003.
793 Lee, C., Martin, R. V., Van Donkelaar, A., Lee, H., Dickerson, R. R., Hains, J. C., Krotkov, N.,
794 Richter, A., Vinnikov, K. and Schwab, J. J.: SO2 emissions and lifetimes: Estimates from
795 inverse modeling using in situ and global, space-based (SCIAMACHY and OMI)

observations, J. Geophys. Res. Atmos., 116(6), 1–13, doi:10.1029/2010JD014758, 2011.
Lelieveld, J., Evans, J. S., Fnais, M., Giannadaki, D. and Pozzer, A.: The contribution of outdoor air pollution sources to premature mortality on a global scale, Nature, 525(7569), 367–371, doi:10.1038/nature15371, 2015.
Masso, C., Nziguheba, G., Mtutegi, J., Galy-Lacaux, C., Wendt, K., Butterbach-Bahl, K., Wairegi, L. and Datta, A.: Soil fertility Managment in Sub-Saharan Africa, in Sustainable Agriculture Reviews, edited by E. Lichtfouse, p. 304, Springer International Publishing., 2017.
Nicholson, S., Some, B., McCollum, J., Nelkin, E., Klotter, D., Berte, Y., Diallo, B., Gaye, I., Kpabeba, G., Ndiaye, O., Noukpozounkou, J., Tanu, M., Thiam, A., Toure, A. and Traore, A.: Validation of TRMM and other rainfall estimates with a high-density gauge dataset for West Africa. Part II: Validation of TRMM rainfall products, J. Appl. Meteorol., 42, 1355–1368, doi:Article, 2003.
Ossohou, M., Galy-Lacaux, C., Yoboué, V., Hickman, J. E., Gardrat, E., Adon, M., Darras, S., Laouali, D., Akpo, A., Ouafo, M., Diop, B. and Opepa, C.: Trends and seasonal variability of atmospheric NO2 and HNO3 concentrations across three major African biomes inferred from long-term series of ground-based and satellite measurements, Atmos. Environ., 207, 148–166, 2019.
Pamela A. Matson, McDowell, W. H., Townsend, A. R. and Vitousek, P. M.: The globalization of N deposition: ecosystemconsequences in tropical environments, Biogeochemistry, 46, 67–83 [online] Available from: http://academic.engr.arizona.edu/HWR/Brooks/GC572-2004/readings/matson.pdf, 1999.
Pommier, M., Law, K. S., Clerbaux, C., Turquety, S., Hurtmans, D., Hadji-Lazaro, J., Coheur, P. F., Schlager, H., Ancellet, G., Paris, J. D., Néďlec, P., Diskin, G. S., Podolske, J. R., Holloway, J. S. and Bernath, P.: IASI carbon monoxide validation over the Arctic during POLARCAT spring and summer campaigns, Atmos. Chem. Phys., 10(21), 10655–10678, doi:10.5194/acp-10-10655-2010, 2010.
Pope, A., Burnett, R., Thun, M., EE, C., D, K., I, K. and GD, T.: Long-term Exposure to Fine Particulate Air Pollution, J. Am. Med. Assoc., 287(9), 1132–1141, doi:10.1001/jama.287.9.1132, 2002.
Raleigh, C., Linke, A., Hegre, H. and Karlsen, J.: Introducing ACLED: An Armed Conflict Location and Event Dataset: Special Data Feature, J. Peace Res., 47(5), 651–660,

827 doi:https://doi.org/10.1177/0022343310378914, 2010.
828 Ramo, R., Roteta, E., Bistinas, I., van Wees, D., Bastarrika, A., Chuvieco, E. and van der Werf,
829 G. R.: African burned area and fire carbon emissions are strongly impacted by small fires
830 undetected by coarse resolution satellite data, Proc. Natl. Acad. Sci. U. S. A., 118(9), 1–7,
831 doi:10.1073/pnas.2011160118, 2021.
832 Robinson, T. P., Wint, G. R. W., Conchedda, G., Van Boeckel, T. P., Ercoli, V., Palamara, E.,
833 Cinardi, G., D'Aietti, L., Hay, S. I. and Gilbert, M.: Mapping the Global Distribution of
834 Livestock, PLoS One, 9(5), e96084, doi:10.1371/journal.pone.0096084, 2014.
835 Roteta, E., Bastarrika, A., Padilla, M., Storm, T. and Chuvieco, E.: Development of a Sentinel-2
836 burned area algorithm: Generation of a small fire database for sub-Saharan Africa, Remote
837 Sens. Environ., 222(November 2018), 1–17, doi:10.1016/j.rse.2018.12.011, 2019.
838 Rufino, M. C., Rowe, E. C., Delve, R. J. and Giller, K. E.: Nitrogen cycling efficiencies through
839 resource-poor African crop-livestock systems, Agric. Ecosyst. Environ., 112(4), 261–282,
840 doi:10.1016/j.agee.2005.08.028, 2006.
841 Sauvage, B., Gheusi, F., Thouret, V., Cammas, J. P., Duron, J., Escobar, J., Mari, C., Mascart, P.
842 and Pont, V.: Medium-range mid-tropospheric transport of ozone and precursors over
843 Africa: Two numerical case studies in dry and wet seasons, Atmos. Chem. Phys., 7(20),
844 5357–5370, doi:10.5194/acp-7-5357-2007, 2007.
845 Stevens, C. J., David, T. I. and Storkey, J.: Atmospheric nitrogen deposition in terrestrial
846 ecosystems: Its impact on plant communities and consequences across trophic levels,
847 Funct. Ecol., 32(7), 1757–1769, doi:10.1111/1365-2435.13063, 2018.
848 Sutton, M. A., Reis, S., Riddick, S. N., Dragosits, U., Nemitz, E., Theobald, M. R., Tang, Y. S.,
849 Braban, C. F., Vieno, M., Dore, A. J., Mitchell, R. F., Wanless, S., Daunt, F., Fowler, D., Blackall,
850 T. D., Milford, C., Flechard, C. R., Loubet, B., Massad, R., Cellier, P., Personne, E., Coheur, P. F.,
851 Clarisse, L., Van Damme, M., Ngadi, Y., Clerbaux, C., Skøth, C. A., Geels, C., Hertel, O., Wichink
852 Kruit, R. J., Pinder, R. W., Bash, J. O., Walker, J. T., Simpson, D., Horváth, L., Misselbrook, T. H.,
853 Bleeker, A., Dentener, F. and de Vries, W.: Towards a climate-dependent paradigm of
854 ammonia emission and deposition, Philos. Trans. R. Soc. B Biol. Sci., 368(1621), 20130166–
855 20130166, doi:10.1098/rstb.2013.0166, 2013.
856 Tian, D. and Niu, S.: A global analysis of soil acidification caused by nitrogen addition,
857 Environ. Res. Lett., 10(2), 024019, doi:10.1088/1748-9326/10/2/024019, 2015.

858 USDA Agricultural Air Quality Task Force: Ammonia Emissions : What To Know Before You
859 Regulate, Washington, DC. [online] Available from:
860 http://www.nrcs.usda.gov/wps/portal/nrcs/detail/national/air/taskforce/?cid=stelprdb1
861 268645, 2014.
862 Vitousek, P., Naylor, R., Crews, T., David, M., Drinkwater, L., Holland, E., Johnes, P.,
863 Katzenberger, J., Martinelli, L. A., Matson, P. A., Nziguheba, G., Ojima, D., Palm, C. A.,
864 Robertson, G., Sanchez, P., Townsend, A. and Zhang, F.: Nutrient Imbalances in Agricultural
865 Development, Science (80-. )., 324, 1519–1520, 2009.
866 Di Vittorio, C. A. and Georgakakos, A. P.: Land cover classification and wetland inundation
867 mapping using MODIS, Remote Sens. Environ., 204(May 2017), 1–17,
868 doi:10.1016/j.rse.2017.11.001, 2018.
869 Vrieling, A., de Beurs, K. M. and Brown, M. E.: Variability of African farming systems from
870 phenological analysis of NDVI time series, Clim. Change, 109(3–4), 455–477,
871 doi:10.1007/s10584-011-0049-1, 2011.
872 De Wachter, E., Barret, B., Le Flochmoën, E., Pavelin, E., Matricardi, M., Clerbaux, C., Hadji-
873 Lazaro, J., George, M., Hurtmans, D., Coheur, P. F., Nedelec, P. and Cammas, J. P.: Retrieval of
874 MetOp-A/IASI CO profiles and validation with MOZAIC data, Atmos. Meas. Tech., 5(11),
875 2843–2857, doi:10.5194/amt-5-2843-2012, 2012.
876 Warner, J. X., Dickerson, R. R., Wei, Z., Strow, L. L., Wang, Y. and Liang, Q.: Increased
877 atmospheric ammonia over the world's major agricultural areas detected from space,
878 Geophys. Res. Lett., 44(6), 2875–2884, doi:10.1002/2016GL072305, 2017.
879 Whitburn, S., Van Damme, M., Kaiser, J. W., Van Der Werf, G. R., Turquety, S., Hurtmans, D.,
880 Clarisse, L., Clerbaux, C. and Coheur, P. F.: Ammonia emissions in tropical biomass burning
881 regions: Comparison between satellite-derived emissions and bottom-up fire inventories,
882 Atmos. Environ., 121, 42–54, doi:10.1016/j.atmosenv.2015.03.015, 2015.
883 World Bank: World Bank Open Data, World Bank Open Data [online] Available from:
884 https://www.data.worldbank.org (Accessed 2 February 2019), n.d.
885 Yegbemey, R. N., Kabir, H., Awoye, O. H. R., Yabi, J. A. and Paraïso, A. A.: Managing the
886 agricultural calendar as coping mechanism to climate variability: A case study of maize
887 farming in northern Benin, West Africa, Clim. Risk Manag., 3, 13–23,
888 doi:10.1016/j.crm.2014.04.001, 2014.

Yokelson, R. J., Christian, T. J., Karl, T. G. and Guenther, A.: The tropical forest and fire emissions experiment: laboratory fire measurements and synthesis of campaign, Rev. Int. Acupunt., 8, 3509–3527, doi:10.1016/s1887-8369(09)71579-0, 2008.

Zheng, B., Chevallier, F., Ciais, P., Yin, Y. and Wang, Y.: On the Role of the Flaming to Smoldering Transition in the Seasonal Cycle of African Fire Emissions, Geophys. Res. Lett., 45(21), 11,998-12,007, doi:10.1029/2018GL079092, 2018.